Local compressibility measurement of the $\nu_{tot} = 1$ quantum Hall state in a bilayer electron system

Ding Zhang,[1] Stefan Schmult,[1] Vivek Venkatachalam,[2] Werner Dietsche,[1] Amir Yacoby,[2]
Klaus von Klitzing,[1] and Jurgen Smet[1]
[1]*Max Planck Institute for Solid State Research, Heisenbergstrasse 1, D-70569 Stuttgart, Germany*
[2]*Department of Physics, Harvard University, Cambridge, Massachusetts 02138, USA*
(Received 22 November 2012; revised manuscript received 19 March 2013; published 10 May 2013)

The filling $\nu_{tot} = 1$ quantum Hall state under charge imbalance is investigated through both transport and thermodynamic measurements on a high-mobility low-density GaAs bilayer sample with negligible single particle tunneling. The $\nu_{tot} = 1$ state demonstrates its robustness against imbalance by evolving continuously from the single layer regime ($\nu_{upper} = 1$, $\nu_{lower} = 0$) to the bilayer regime with fillings $\nu_{upper} = 1/3$ and $\nu_{lower} = 2/3$ for the separate layers. The energy gap of the $\nu_{tot} = 1$ state obtained from compressibility measurements using single electron transistors depends on position, i.e., the local disorder potential. Nevertheless, compressibility and thermal activation measurements yield comparable values for the energy gap under imbalance.

DOI: 10.1103/PhysRevB.87.205304 PACS number(s): 73.43.Nq, 71.27.+a, 73.43.Qt

I. INTRODUCTION

In two closely spaced two-dimensional electron systems (2DES), a condensate of electron-hole pairs[1] forms when both layers are at half filling and the interlayer Coulomb interactions (e^2/d, d is the layer separation) become comparable to the intralayer Coulomb interactions (e^2/l_B, l_B is the magnetic length). This excitonic condensate manifests itself in transport as an incompressible quantum Hall (QH) state[2,3] at total filling factor $\nu_{tot} = \nu_{upper} + \nu_{lower} = 1$ with Hall resistance quantization and vanishing longitudinal resistance. A plethora of interaction phenomena has been unveiled at $\nu_{tot} = 1$. For example, the interlayer tunneling bears a striking resemblance to the I-V characteristic of a Josephson junction.[4–6] A Goldstone mode coming from the spontaneous breaking of the U(1) symmetry has been confirmed.[7] In transport, the existence of excitonic superfluidity at $\nu_{tot} = 1$ has been uncovered in a counterflow configuration.[8–10]

Intensive efforts have been devoted to investigate the energy gap of the $\nu_{tot} = 1$ QH state. The dependence of the energy gap on charge imbalance[10–14] as well as on the pseudo-[15] and real-spin[16,17] polarizations has been explored. Theoretically, it is expected that the $\nu_{tot} = 1$ QH state is robust against a charge imbalance. This robustness has been established in a bilayer hole system by Clarke *et al.*[18] Similar investigations have been carried out on bilayer electron systems with large single-particle tunneling.[12,13] Excitonic superfluidity, however, was only demonstrated on electron-electron bilayer samples with negligible single-particle tunneling.[8–10] Those samples have only been studied in a limited range of imbalance.[10,14] Therefore, a complete study of the $\nu_{tot} = 1$ QH state under charge imbalance in samples hosting most of the exotic phenomena associated with an excitonic condensate is still lacking. Additionally, past studies of the energy gap at $\nu_{tot} = 1$ were based solely on thermally activated transport instead of measuring directly the discontinuities in the chemical potential.

In this work, we address the energy gap of the $\nu_{tot} = 1$ state by measuring the local inverse compressibility $\chi^{-1} = n^2 \partial\mu/\partial n$ using a single-electron transistor (SET).[19] In our bilayer sample with a structure that has produced Josephson-like tunneling[20] and excitonic superfluidity,[21] the $\nu_{tot} = 1$ QH state evolves continuously over the whole range of charge imbalance. At the base temperature of a dilution refrigerator (20 mK), we extract the discontinuity in the chemical potential $\Delta\mu$ for the $\nu_{tot} = 1$ quantum Hall state. We compare the evolution of $\Delta\mu$ with the energy gap E_g determined from thermal activation. Finally, despite the difficulties posed by the deeply buried low-density bilayer system, we were able to observe the localization of charged quasiparticles at $\nu_{tot} = 1$.

II. SAMPLE

Our bilayer samples are fabricated on a double quantum well GaAs/Al_xGa_{1-x}As heterostructure grown by molecular beam epitaxy. A schematic of the sample is displayed in Fig. 1. The heterostructure is composed of a 200-nm Si-doped GaAs layer, which serves as the backgate, followed by a 200-nm-thick low temperature grown GaAs layer and a buffer layer with a total thickness of 1660 nm. Two 19-nm GaAs quantum wells separated by a 9.6-nm AlAs/GaAs superlattice barrier were placed on top of this barrier. The quantum wells were covered by a 450-nm $Al_{0.23}Ga_{0.77}As$ spacer layer and then a 40-nm Si doped $Al_{0.23}Ga_{0.77}As$ layer.[22] Finally, a 200-nm AlGaAs layer plus a 20-nm capping layer terminated the growth. For double quantum well structures, the symmetric-antisymmetric subband splitting Δ_{SAS} characterizes the single-particle interlayer tunneling. For our sample, Δ_{SAS} was estimated to be 150 μK.[20]

Hall bars with a width of 400 μm were patterned using optical lithography and wet chemical etching. SETs were then evaporated on the Hall bar mesa. The SET consists of a 80×500 nm^2 aluminum island with tunnel contacts to two aluminum electrodes.[23] Two Hall bar samples with these stationary SETs were measured in a 20-mK ^{3}He-^{4}He dilution refrigerator. Similar results from both the transport and the SET measurements were observed on all samples, so we will focus on one sample with three SETs for the remainder of this paper. The upper quantum well has an intrinsic electron density (n_u) as low as 1.7×10^{10} cm^{-2}, whereas the lower quantum well has no electrons when no backgate voltage is applied ($V_{BG} = 0$ V): $n_l = 0$. The mobility is above 1.1×10^6 cm^2/V s within the density range: $n = n_u + n_l = 1.7$–6.9×10^{10} cm^{-2}.

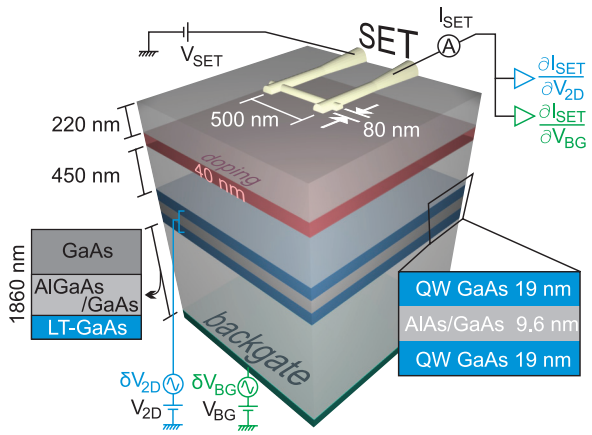

FIG. 1. (Color) A schematic of the sample, the aluminum SET and the circuitry for the compressibility measurement. The SET consists of an 80 × 500-nm^2 aluminum bar connected by two electrodes.

III. TRANSPORT

We start by showing the transport results. Standard low-frequency ac lock-in techniques were employed with a 1-nA ac current oscillating at 8 Hz. By increasing the backgate voltage (V_{BG}), we were able to tune the system from a single layer to a bilayer. A color rendition of the longitudinal resistance in the density (n) versus magnetic field (B) plane is plotted in Fig. 2. White numbers mark total filling factors, yellow numbers indicate the filling factor of the upper layer. We focus on the $\nu_{tot} = 1$ QH state first and explain other features at the end of this section.

The $\nu_{tot} = 1$ QH state is unique, since it is the only incompressible state evolving continuously along a straight line from the single layer to the bilayer QH state without any interruption, i.e., it survives independent of the degree of charge imbalance. Other QH states do not possess this property. The regions where the Hall resistance plateau is at $h/2e^2$, for example, are separated by high resistance regions. In the region where $B \in [1,2]$ T and $V_{BG} \in [0.4,0.7]$ V, the $\nu = 1$ QH state is drastically enhanced. Both the longitudinal resistance minimum as well as the Hall plateau extend over a much wider range of the magnetic field. Temperature dependent transport studies suggest that both the single layer $\nu_{upper} = 1$ QH state and the bilayer $\nu_{tot} = 1$ QH state induced by interlayer correlations are simultaneously present. The gray shaded region in Fig. 2(a) marks, for instance, $\nu = 1$ quantum Hall behavior at a temperature of 850 mK. At this elevated temperature, the $\nu_{tot} = 1$ QH state can be distinguished from

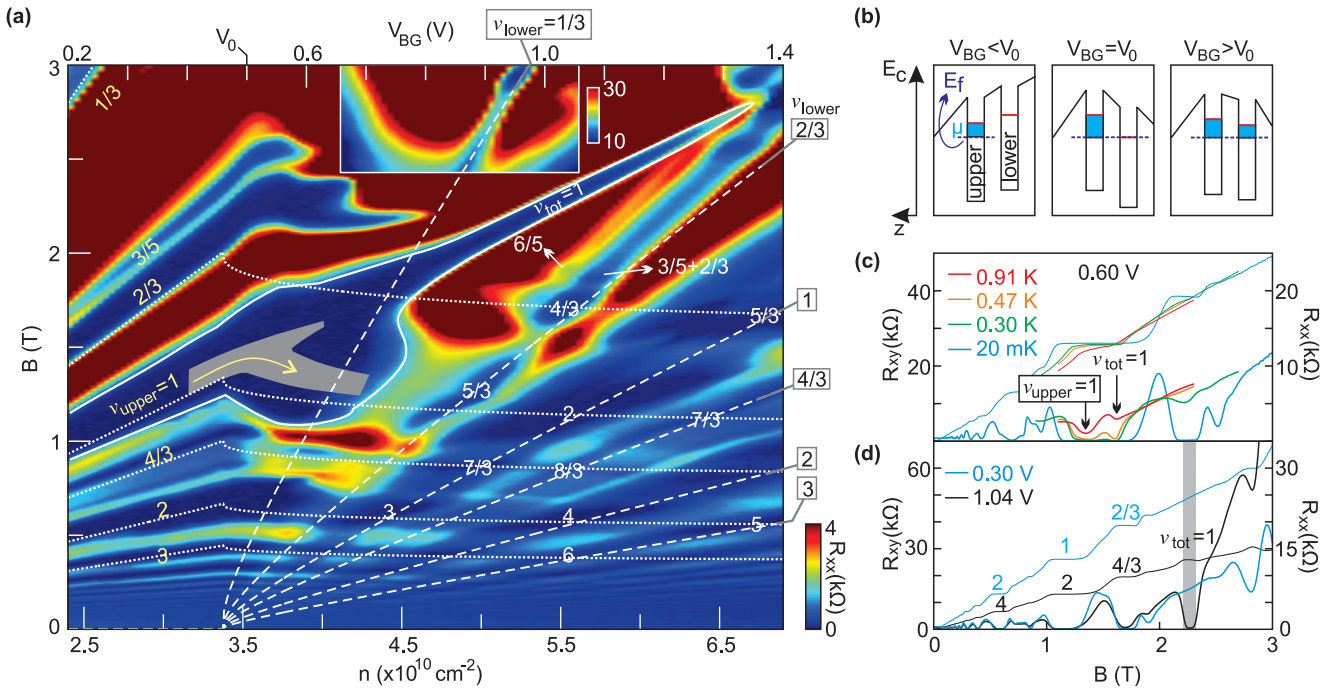

FIG. 2. (Color) (a) Color rendition of the longitudinal resistance R_{xx} as a function of magnetic field B and backgate voltage V_{BG}. On the bottom axis also the total density n has been plotted. Total filling factors ν_{tot} are denoted in white numbers. They are determined from the height of the QH plateaus in the R_{xy} traces. The QH state at $\nu_{tot} = 3/5 + 2/3$ corresponds to $\nu_{upper} = 3/5$ and $\nu_{lower} = 2/3$. Dotted (dashed) lines mark the B-field positions where the upper (lower) layer is expected to condense in a quantum Hall state. Lines are plotted for $\nu_{upper,lower} = 1/3$, 2/3, 1, 4/3, 2, and 3. They were theoretically calculated with two fitting parameters. Solid lines highlight the region where $\nu = 1$. Gray color marks the same $\nu = 1$ region but at 850 mK with the arrow indicates the bending of the $\nu_{upper} = 1$ QH state. (b) Schematic drawings of the conduction band profile at different backgate voltages. The Fermi level is drawn below the subband to emphasize that the chemical potential is negative for a low-density 2DES. In order to fill the lower quantum well, one has to align the lowest subband of the lower quantum well with the Fermi level. This alignment requires a backgate voltage of V_0. (c) Hall (R_{xy}) and longitudinal (R_{xx}) resistances as a function of magnetic field for V_{BG} =0.6 V at different temperatures. Two minima can be observed in the R_{xx} traces in the region where $\nu = 1$. These minima are attributed to the single layer $\nu = 1$ and the correlated $\nu_{tot} = 1$ QH states, respectively. (d) Comparison between the Hall and longitudinal resistance traces taken at $V_{BG} = 0.30$ V, where only the upper layer is populated, and at $V_{BG} = 1.04$ V, where the two layers are balanced.

the $\nu_{upper} = 1$ state. The coexistence of both $\nu = 1$ QH states can also be seen in the longitudinal resistance traces recorded at elevated temperatures in Fig. 2(c). The single wide plateau at low temperatures indicates a large number of localized states in this region. At still higher backgate voltages (around $V_{BG} = 1.04$ V), when both layers are nearly equally populated, all integer and fractional quantum Hall states have even numerators with one exception: the $\nu_{tot} = 1$ QH state [shown in Fig. 2(d)]. The energy gap E_g at $\nu_{tot} = 1$ obtained from thermal activation is large for such a correlated state. The robustness of the $\nu_{tot} = 1$ QH state is also confirmed in the SET measurements. We compare the energy gaps with the discontinuity in the chemical potential in Sec. IV C. Here we point out that in the balanced case E_g is above 1 K. In the imbalanced case with small d/l_B ratio E_g exceeds 6 K (higher gap values are difficult to determine in a dilution refrigerator). These values are higher than the previously reported values at similar d/l_B values.[9–11,14,17,24] This large energy gap is a result of the improved sample quality. By further adding electrons to the bilayer system, the ratio d/l_B increases and the intralayer interactions start to dominate. As the energy gap closes, the system behaves more and more as two separate layers and the $\nu_{tot} = 1$ QH state eventually collapses.

Concomitant with the disappearance of the $\nu_{tot} = 1$ QH state, regions with low resistances emerge in the close vicinity of $\nu_{tot} = 1$ [upper right corner of Fig. 2(a)], but it is difficult to assign specific fractional filling factors. The low resistance region centered around ($B = 2.5$ T, $V_{BG} = 1.35$ V) is accompanied by a plateau in the Hall trace but with a height slightly higher than the plateau at $\nu_{tot} = 1$ (the difference is about 500 Ω). For the regions at either higher magnetic fields or higher gate voltages, the Hall traces do not show any pronounced plateaus.

In order to make the paper self-contained and to introduce the concept of compressibility, we take a closer look at other features observed in Fig. 2(a). Up to $V_{BG} = V_0 \cong 0.5$ V (marked on the top axis), the system behaves as a single layer and the QH states shift linearly to higher B fields with increasing backgate voltage. A schematic of the conduction band profile for the case $V_{BG} < V_0$ is displayed in the left panel of Fig. 2(b). To occupy the second quantum well, the band bending needs to be overcome in order to achieve alignment among the lowest subbands of the two quantum wells. This alignment occurs at approximately $V_{BG} = V_0$ [middle panel, Fig. 2(b)]. Since we are operating at low carrier densities, the 2DES possesses a negative compressibility.[25] Hence not only electrostatic band bending, but also the reduction of the chemical potential while adding electrons to the upper quantum well needs to be compensated in view of the negative compressibility before the subbands of the adjacent quantum wells align. When the lower quantum well becomes populated, the QH states associated with the upper layer drop to lower magnetic field values in the region $V_{BG} = 0.5$–0.6 V. This too is a signature of negative compressibility. The density in the upper layer decreases and is transferred to the lower layer because it is energetically more favorable to occupy the lower layer with a larger density.[11,26–28] This can also be viewed as a result of overscreening of the lower 2DES, so that the number of electric field lines reaching the upper layer decreases. This electron interaction effect can be modeled by treating two ideally thin 2DES within the Hartree-Fock approximation (see the calculation in Appendix A). The dashed and dotted lines in Fig. 2(a) are from our calculations. They represent the B-field positions of the QH states for the individual layers. As the two layers enter incompressible ground states with different filling factors, a composite QH state appears with the plateau at $R_{xy} = h/(\nu_{upper} + \nu_{lower})e^2$, where ν_{upper} and ν_{lower} are quantum Hall filling factors of the upper and lower layers. Our results are consistent with previous observations on a hole-hole bilayer.[11,18] For $\nu \geqslant 1$, the theoretically calculated positions of the integer and fractional quantum Hall states fit well with the experimental data. The main discrepancy is the bending point of the trace for $\nu_{upper} = 2/3$. Also, the trace for $\nu_{lower} = 2/3$ deviates from the region where R_{xx} shows a minimum ($B \in [2,3]$ T, $V_{BG} \in [1.0,1.4]$ V). It indicates that in the quantum limit where the electrons are squeezed into the lowest Landau level our simple model is no longer satisfactory.[29] We will return to this point in Sec. IV B.

IV. SET MEASUREMENT

A. Measuring principle

To probe the local thermodynamic behavior of the 2DES a single-electron transistor is used.[19] We will first describe the technique for a single layer (or a bilayer that behaves as a single layer). An electric field δE_{BG} generated by varying the backgate voltage pushes charges into or out of the 2D system. Because of the finite density of states, this δE_{BG} modifies the chemical potential by an amount $\delta\mu$. A part of the electric field δE_1 penetrates through the layer and is detected by the SET. δE_1 causes a detectable change in the current flowing through the SET (δI_{SET}) when it is operated at a suitable working point. Therefore, δI_{SET} reflects the change of the chemical potential in the 2DES through the following chain of quantities:

$$\delta\mu \Rightarrow \delta E_1 \Rightarrow \delta I_{SET}. \tag{1}$$

This change in the chemical potential is related to the backgate modulation δV_{BG} according to the equation

$$\delta\mu = \left(\frac{\partial\mu}{\partial n}\right)\left(\frac{\partial n}{\partial V_{BG}}\right)\delta V_{BG}. \tag{2}$$

Here, $\partial\mu/\partial n$ is just the inverse compressibility divided by n^2. The conversion factor from $\delta\mu$ to δI_{SET} can be determined by calibrating the SET response. To this end, the electrochemical potential of the 2DES (δV_{2D}) is changed directly and the induced change in the SET current (δI_{SET}) is measured. $\delta I_{SET}/\delta V_{2D}$ is referred to as the sensitivity of the SET. Hence, in the experiment, two ac signals are simultaneously applied (shown in Fig. 1): (1) The backgate oscillates with an amplitude δV_{BG} at a frequency f_{BG}. (2) The electrochemical potential of the 2D system oscillates with an amplitude δV_{2D} at a frequency f_{2D}. The induced SET current contains both frequency components and yields the quantities $\delta I_{SET}/\delta V_{2D}$ and $\delta I_{SET}/\delta V_{BG}$. We define

$$\eta = \frac{\delta I_{SET}}{\delta V_{BG}}\left(\frac{\delta I_{SET}}{\delta V_{2D}}\right)^{-1}. \tag{3}$$

A detailed derivation given in Appendix B yields the following relationship between the measured quantity in experiment η

and the inverse compressibility χ^{-1} or $\frac{\partial\mu}{\partial n}$:

$$\eta = \frac{\varepsilon}{e^2 l_{BG}} \frac{\partial \mu}{\partial n} = \frac{\varepsilon}{e^2 l_{BG}} \frac{\chi^{-1}}{n^2}. \tag{4}$$

Here, l_{BG} is the distance from the backgate to the quantum well, and ε is the dielectric constant. l_{BG} can be experimentally obtained by extracting the density from the Hall resistance or Shubnikov–de Haas oscillations as a function of the backgate voltage. By measuring η it is possible to determine the inverse compressibility of a single 2DES. The same approach was also employed recently in experiments on bilayer graphene.[30] Henriksen and Eisenstein[31] also determined the compressibility of bilayer graphene using a capacitive arrangement based on the same principle.

Equation (4) is valid as long as the bilayer acts as a strongly coupled system. For our GaAs bilayer system, however, the data we present indicates that this condition is satisfied only when the $\nu_{tot} = 1$ QH state forms. It demonstrates the strong coherence of the bilayer at this total filling factor. The exchange of electrons between the layers becomes very unlikely out of the coherent regime and the single-particle tunneling is limited by the extremely small Δ_{SAS}. Therefore, inverse compressibility components for the individual layers are well defined when the system is not in the $\nu_{tot} = 1$ state. In this case, the backgate controls the density in the lower quantum well (n_l) directly, whereas the density variation in the upper quantum well (δn_u) is induced via the interlayer electric field (δE_{int}). δE_{int} reflects the change of the chemical potential in the lower quantum well ($\delta\mu_l$). Writing down the relations between these quantities yields

$$\delta I_{SET} \Leftarrow \delta\mu_u = \left(\frac{\partial \mu_u}{\partial n_u}\right) \delta n_u, \tag{5}$$

$$\delta n_u \Leftarrow \delta E_{int}, \tag{6}$$

$$\delta E_{int} \Leftarrow \delta\mu_l = \left(\frac{\partial \mu_l}{\partial n_l}\right) \left(\frac{\partial n_l}{\partial V_{BG}}\right) \delta V_{BG}. \tag{7}$$

One can readily see that by monitoring δI_{SET} we measure the *product* of the two compressibility components in a bilayer (details shown in Appendix B):

$$\eta = \frac{\delta I_{SET}}{\delta V_{BG}} \left(\frac{\delta I_{SET}}{\delta V_{2D}}\right)^{-1} = \frac{d_u d_l}{l_{BG}(d + d_u + d_l) + d d_l}. \tag{8}$$

Here, d is the center-to-center distance between the two quantum wells and $d_i = \frac{\varepsilon}{e^2} \frac{\partial \mu_i}{\partial n_i}$, $i = u$ or l denoting the upper or the lower layer. l_{BG} is now the distance from the backgate to the lower 2DES.

Measurements were carried out with an ac voltage to the backgate of 10 mV ($\sim$4 electrons μm^{-2} are added and removed again during one cycle), at 1.7 Hz or 1 mV at 11 Hz. The amplitude and the frequency were kept low to minimize resistive effects.[19] Measurements with the larger amplitude $\delta V_{BG} = 10$ mV enable us to determine the discontinuity of the chemical potential ($\Delta\mu$) at $\nu_{tot} = 1$. In order to investigate discrete charging events near $\nu_{tot} = 1$ a smaller amplitude is required to prevent too many simultaneous charging events. We note that the large distance between the SET and the deeply buried 2DESs significantly reduces the spatial resolution. As a result single discrete charging events are more difficult to detect than in shallower 2DESs. The ac voltage applied to the two 2DESs for calibration purposes was 0.1 mV at 26 Hz.

B. Inverse compressibility

Figure 3(a) plots the measured quantity η at zero magnetic field and compares it to our calculations. A sign reversal of η occurs at a backgate voltage of about 0.45 V and is correctly explained by Eq. (8). For a single 2DES with low density, the compressibility is negative and hence η is negative. When a bilayer forms, both layers exhibit negative compressibility and the product yields a positive result, which accounts for the sign reversal. The calculation (dotted line) fits reasonably well with the data. When the bilayer has formed, some deviation between theory and experiment becomes apparent. The theoretical curve quickly drops close to zero, while the experimental data fluctuate around a nonzero constant value. We attribute this difference to band-bending effects[25] which are not considered in our simple model.

Figure 3(a) also displays η measured at $B = 2.3$ T. Apart from the extrema caused by the condensation of one or both

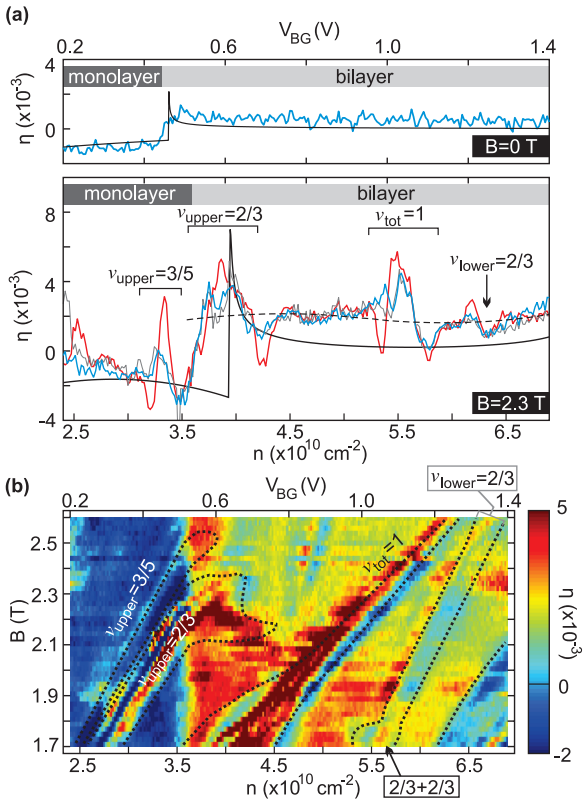

FIG. 3. (Color) (a) η vs the averaged density n. The blue traces were obtained using the same SET at $B = 0$ T (top panel) and $B = 2.3$ T (bottom panel), respectively. The red and gray traces were obtained from the other two SETs at $B = 2.3$ T. The solid black lines are from the theoretical calculations. The dashed black curve illustrates the smoothed background for the data represented by the red curve. This background was later subtracted from the original data to determine $\Delta\mu$ at $\nu_{tot} = 1$. (b) η plotted as a function of the magnetic field and the density. The dotted black lines separate QH states identified from transport.

layers into an incompressible QH state, we point out one generic feature for the curve in the presence of a B field: The position where the jump from $\eta < 0$ to $\eta > 0$ occurs shifts to higher density compared to the zero-field case. This is also seen in the transport data [compare the bending points for $\nu_{upper} = 2/3$ and $\nu_{upper} = 1$ in Fig. 2(a)]. It stems from the enhancement of the negative inverse compressibility in the quantum limit.[32] Increasing the density in the upper quantum well results in a stronger decrease of the chemical potential compared to the $B = 0$ T case. Therefore, one has to apply a higher backgate voltage in order to pull down further the lowest subband in the lower quantum well and make it align with E_F.

This observed behavior in a magnetic field can be qualitatively explained in our simple model. For calculating the inverse compressibility, we use the density dependence of the total energy of electrons described by Fano and Ortolani.[32] The outcome is shown as the solid black line in Fig. 3(a). The rapid jump of η to positive values has indeed shifted to higher densities. A more complete theoretical description should include the band-bending effect in a self-consistent manner.

We now examine the regions where QH states emerge. We focus on Fig. 3(b). In the single layer regime, η is mostly negative (dark blue) but develops a peak whenever the two-dimensional electron gas condenses into a QH liquid. The system has become incompressible. Features corresponding to the $\nu_{upper} = 3/5$ and $2/3$ quantum Hall states can be observed. In the bilayer regime, η turns positive as it contains the product of the negative inverse compressibility of each layer. When one layer condenses into an incompressible quantum Hall fluid, the compressibility of that layer reverses sign, turns positive, giving rise to an overall negative numerator in Eq. (8). Hence, η develops a dip rather than a peak. This expected behavior is nicely illustrated in Fig. 3(b) for $\nu_{lower} = 2/3$. The dotted curves in the graph indicate the boundaries where quantum Hall behavior is observed in transport. In the region where the lower layer is in the $\nu_{lower} = 2/3$ QH state while the upper layer is still compressible, η has a minimum. In contrast, when both layers condense into a fractional QH state, η develops a maximum. For example, at the bottom of Fig. 3(b) a small peak is visible at $B = 1.75$ T and $V_{BG} = 1.1$ V when $\nu_{upper} = \nu_{lower} = 2/3$.

As we sweep the density, η displays a peak when the system approaches $\nu_{tot} = 1$. In this range, the bilayer acts as a single incompressible layer. The system can be described by Eq. (4), where μ and n refer to the total chemical potential and the total density, respectively. The peak at $\nu_{tot} = 1$ in Fig. 3(a) is flanked by two minima. These minima are reminiscent of the diverging compressibility previously reported in a single layer due to the interaction among quasiparticles which form as we move from exact integer or fractional filling factor.[25,33] Since we measure compressibility locally, a scan of the density or magnetic field around $\nu_{tot} = 1$ may give rise to multiple peaks. Local density variations can cause the formation of the $\nu_{tot} = 1$ at somewhat different densities or fields in the region sensed by the SET. If two regions of different density are close enough to the SET, two peaks may be detected. This effect is manifested in the blue trace in Fig. 3(a) at $B = 2.3$ T. The position of the compressibility maximum recorded with different SETs varies somewhat, reflecting the density fluctuations and the local nature of our measurement.

C. Energy gaps at $\nu_{tot} = 1$

Charge excitations at $\nu_{tot} = 1$ involve quasiparticles referred to as merons.[34–36] They are vortices whose charge depends on the imbalance: $|e^*/e| = \nu_{u,l}$. Four different types can be distinguished according to their vorticity and the interlayer polarization. Wiersma *et al.* have experimentally shown that the behavior of the activation energy E_g at $\nu_{tot} = 1$ under imbalance depends crucially on the layer through which the current is imposed.[10] When measuring by driving current through a single layer only (drag experiment), the activation energy E_g exhibits an asymmetric dependence on the degree of imbalance. If current is passed through both layers simultaneously, the activation energy displays a parabolic dependence with the minimum located at the balanced point.[14] These apparently contrasting behaviors were later explained theoretically by Roostaei *et al.*[35] If only a single layer carries current, only two out of the four types of merons are subject to an external force. They cause dissipation in the drive layer only and the activation energy depends assymetrically on the imbalance. Since measurements of the chemical potential proceed without passing current through the sample, it is of interest to investigate the energy gaps extracted from the discontinuity in the chemical potential ($\Delta\mu$) at $\nu_{tot} = 1$. We extract $\Delta\mu$ with the following procedure. First, a smoothed background is subtracted from the raw data [see Fig. 3(a)]. Subsequently, η is integrated over the density n. Here, n is not the local density but the density obtained from transport measurements. Scaled by a geometrical factor, the height between the local minimum and maximum of the integrated curve around $\nu_{tot} = 1$ yields $\Delta\mu$.[37] Since η was measured by fixing B and sweeping V_{BG}, $\Delta\mu$ was determined at fixed B fields. We converted the B axis to a density axis by using $\nu_{tot} = 1$, i.e., $n = eB/h$.

In Fig. 4, we compare $\Delta\mu$ with the energy gap E_g derived from thermal activation experiments when the current is sent through both layers: $R_{xx,min} = R_0 e^{-E_g/2kT}$. Here we define the imbalance as $2\Delta n/n_0 = 2(n - n_0)/n_0$, where $n_0 = 5.5 \times 10^{10}$ cm^{-2} is the total density when the two layers are balanced. The thermal activation gap measured in this configuration is expected to increase parabolically with imbalance at fixed total density, i.e., d/l_B fixed.[10,14] This parabolic dependence is not observed here, because the total density is not fixed. Here, we go along the $B = nh/e$ line so that not only the imbalance but also the ratio d/l_B is changed. The $\nu_{tot} = 1$ QH state is strengthened as d/l_B decreases. In the range where $2\Delta n/n_0 < 0$, increasing the density drives the system to balance and also shifts the QH state to higher B fields. The latter causes an increase of d/l_B. Both account for a decrease of E_g. In the region where $2\Delta n/n_0 > 0$, the weakening of the interlayer interactions due to a larger d/l_B appears to play a larger role than the stabilizing effect brought about by the charge imbalance. As a result, E_g continues to decrease.

The discontinuity in the chemical potential at $\nu_{tot} = 1$ obtained from different SETs follows overall the same decreasing trend as the thermal activation gap. In the SET measurement, the excitations are induced only through δV_{BG}. Naively δV_{BG}

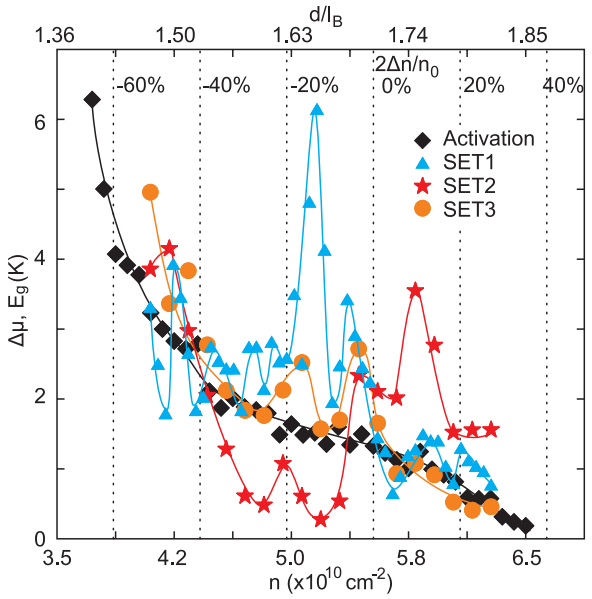

FIG. 4. (Color) $\Delta\mu$ and E_g at $\nu_{tot} = 1$. Data points denoted by SET1, SET2, and SET3 are derived from the compressibility data of three different SETs on the same sample. The black squares represent E_g determined from thermal activation. Lines are guides to the eye.

adds charges to the lower layer only and one might expect to see solely excitations from the lower layer. The expected result in this case would be that $\Delta\mu$ increases with increasing n. However, Fig. 4 shows that $\Delta\mu$ overlaps with E_g quite well even at large imbalance. Since E_g is determined when both layers are participating in the transport, this overlap indicates that for the chemical potential jump at $\nu_{tot} = 1$ merons in both layers are involved. The strong coherence makes the layers indistinguishable and we are dealing with paired merons just as in the activation experiment with current imposed through both layers.[35,36]

We now turn to the nonmonotonic behavior of $\Delta\mu$. Data from SET1 shows a significant peak around 5.2×10^{10} cm^{-2}. We attribute this strong peak to the fact that two incompressible regions are contributing to the SET signal. This is evident also from the incompressible behavior in the $\nu_{upper} = 2/3$ region in Fig. 3(b) (blue and gray traces from two different SETs). Despite this complication, one can see that the energy gap varies significantly with position. The spatial variation in $\Delta\mu$ is likely related to a variation in the disorder potential. A larger energy gap from the SET data indicates a locally cleaner area. In principle, it is possible to determine the charge of the quasiparticles e^* by using the equation $\Delta\mu = |e/e^*|E_g$. Dorozhkin *et al.* determined the quasiparticle charge at 1/3 by comparing $\Delta\mu$ from capacitance measurement with E_g.[33] Since in our case $\Delta\mu$ is strongly affected by local disorder, this equation is of limited use. Nevertheless, the fact that most of the data points overlap seems to suggest that $e/e^* = 1$. This analysis again points to our previous assertion that merons come as pairs in our system.

D. Discrete charging at $\nu_{tot} = 1$

A more accurate approach to determine the charge of quasiparticles is to use the SET for studying charge

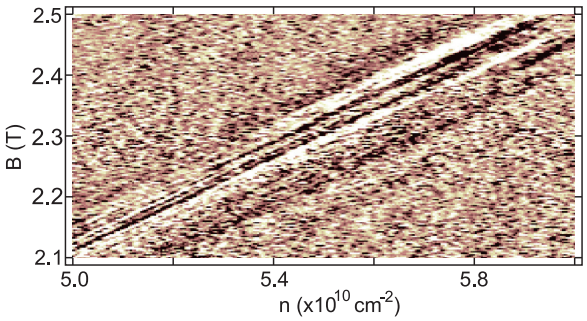

FIG. 5. (Color) The local inverse compressibility at $\nu_{tot} = 1$ plotted as a function of the average density and the magnetic field. A smoothed background has been subtracted to highlight the discrete charging lines (black).

localization.[23,38,39] In general, charge carriers will redistribute and generate a spatially varying density profile in an attempt to screen the bare disorder potential. As long as the local density of states is not exhausted, they are able to accomplish this task. As a Landau level approaches complete filling in some regions, the required density to flatten the bare disorder potential locally exceeds the level degeneracy. Hence, the bare disorder potential cannot be screened away everywhere and an incompressible lake with compressible islands emerges. The discrete nature of charge becomes relevant. Elementary charge excitations can be added to the remaining compressible dots only one at a time when the overall density is raised sufficiently. Each charging event corresponds to filling a localized state and when the SET is close by, this charging event gives rise to a jump in the local chemical potential and is detected as a spike in the local compressibility. As the average density is increased further, more and more charges are added to the dots each time producing a spike in the compressibility. The same landscape of compressible areas appears at a higher B. Assuming a fixed charge, the same charging physics recurs at the same density deviation from complete filling. The filling of a specific localized state therefore produces in the density vs magnetic field plane a line with a slope equal to the filling factor of the underlying quantum Hall state. For the $\nu_{tot} = 1$ state a more complex behavior is expected. If individual merons are detected, the spacing between the charging spikes should change with the degree of imbalance and charging lines would no longer be parallel to filling factor 1. If, however, quasiparticles are added to a compressible dot in pairs, parallel lines are expected instead like for conventional quantum Hall states, since paired merons carry a fixed total charge equal to the electron charge.

In our bilayer sample, investigating the charge localization is challenging as the 2DES is deeply buried below the surface. The SET couples to a large area such that many charging events occur simultaneously and some averaging is inevitable. Still, by reducing the excitation voltage δV_{BG}, several charging lines at $\nu_{tot} = 1$ were observed (see Fig. 5). Even though the experiment in Fig. 5 exhibits parallel lines and would therefore suggest charge localization physics based on paired merons, caution is due to draw this conclusion. Simulations show that the width of the charging lines is so large that it is not possible to distinguish the case with fixed charge e for charging with

paired merons or variable charge if individual merons are added to the system. For such charge localization experiments, an improved spatial resolution is quintessential. This requires shallower bilayer systems while keeping the density low in order to still satisfy $d/l_B < 2$ for the $\nu_{tot} = 1$ QH state. Lowering the aluminum content used for the spacer between the 2DES and the doping layer is one possible solution.

V. CONCLUSION

In conclusion, we observed a continuous evolution of the $\nu_{tot} = 1$ QH state out of the single layer $\nu = 1$ QH state in a low-density bilayer with a mobility exceeding 1.1×10^6 cm^2/V s. We employed an SET to investigate the chemical potential discontinuity $\Delta\mu$ at $\nu_{tot} = 1$. As the SET probes a local area, the evolution of $\Delta\mu$ as a function of charge imbalance and d/l_B is greatly influenced by the disorder potential. The charging of localized states was observed at different values of the charge imbalance at $\nu_{tot} = 1$. From a comparison between the density dependence of the jump in the chemical potential and the activation energy in transport, we conclude that the charged quasiparticles or merons probed in such experiments at $\nu_{tot} = 1$ are paired.

ACKNOWLEDGMENTS

We thank Johannes Nübler, Benedikt Friess, Xuting Huang, Timo Hyart, and Bernd Rosenow for helpful discussions. We acknowledge financial support from the German Ministry of Science and Education (BMBF).

APPENDIX A: CALCULATING $n(V_{BG})$

In a case where the lower layer is completely depleted, the negative compressibility has little influence on the density in the upper layer. The density scales almost linearly with V_{BG}. When both layers are occupied, the equations for modeling the bilayer are as follows:[25]

$$eV_{dop} - \mu_u - eV_{2D} = eE_1 l_{FG}, \tag{A1}$$

$$\mu_u - \mu_l = eE_{int} d, \tag{A2}$$

$$eV_{BG} - \mu_l - eV_{2D} = eE_2 l_{BG}, \tag{A3}$$

$$E_1 - E_{int} = \frac{e}{\varepsilon} n_u, \tag{A4}$$

$$E_{int} + E_2 = \frac{e}{\varepsilon} n_l. \tag{A5}$$

The meaning of the electric fields E_1, E_2, and E_{int}, the distances l_{FG}, l_{BG}, and d, and the chemical potentials μ_u and μ_l is illustrated in the inset of Fig. 6. V_{2D} is the voltage applied to the two 2DESs. V_{dop} is a fitting parameter used to characterize the intrinsic electron density when all applied voltages equal zero. For the curves plotted in Fig. 2(a) and Fig. 6, we used $V_{dop} = 0.178$ V.

Since the two layers are grounded, we set $V_{2D} = 0$. Using Eqs. (A1), (A2), and (A4), it is possible to remove E_1 and E_{int} and we obtain

$$en_u = \frac{\varepsilon}{l_{FG}} V_{dop} + \frac{\varepsilon}{d}\frac{\mu_l}{e} - \frac{\varepsilon(l_{FG}+d)}{l_{FG} d}\frac{\mu_u}{e}. \tag{A6}$$

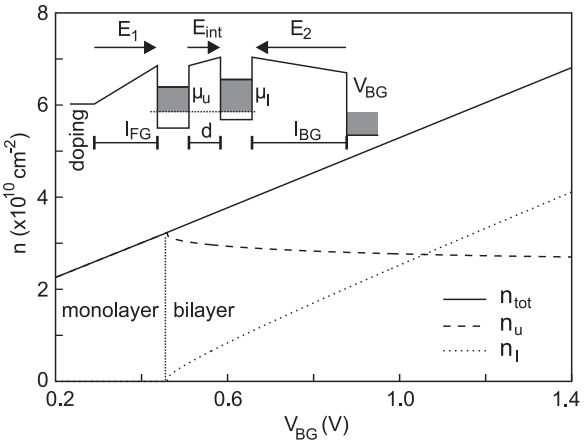

FIG. 6. Densities as a function of the backgate voltage calculated for $B = 0$ T. The inset shows the conduction band profile of the bilayer system. We took the growth parameters $l_{FG} = 450$ nm and $d = 28.6$ nm. l_{BG} is experimentally determined to be 1780 nm from the linear fitting of the total density as a function of V_{BG} (we used a relative dielectric constant of 12.25 for $Al_{0.23}Ga_{0.77}As$).

Equation (A6) reflects that the charge density in the upper layer is determined by the capacitive coupling to the doping layer (first term on the right-hand side), the capacitive coupling to the lower layer (second term), and the quantum capacitance (third term).

For $B = 0$, we employ the results from the Hartree-Fock approximation to describe the chemical potential as a function of the electron density:

$$\mu_i(n_i) = \frac{\hbar^2\pi}{m} n_i - 2\sqrt{\frac{2}{\pi}}\frac{e^2}{4\pi\varepsilon}\sqrt{n_i}, \qquad i = u,l. \tag{A7}$$

Instead of determining $n_{u,l}$ as a function of V_{BG}, we fix the value of n_l and calculate the required V_{BG}. With the help of Eq. (A7) for $i = l$ we obtain μ_l. Putting the value of μ_l into Eq. (A6), n_u and μ_u can then be determined by solving Eq. (A6) together with Eq. (A7) for $i = u$. Based on these results, the required value of V_{BG} is calculated.

If only the upper layer is occupied, it is necessary to modify Eqs. (A1)–(A5) for the single layer case in order to calculate n_u as a function of V_{BG}. Plotting n_u and n_l as a function of $V_{BG} + 0.335$ V (see Fig. 6), the theoretical curves fit well with the experimental data. The offset voltage 0.335 V is necessary to account for the band-bending effect. (We linearly extrapolated the calculated data to the region [0,0.335] V.)

For $B = 2.3$ T, we used the "backbone" function[32] to describe $\mu_u(n_u)$ and $\mu_l(n_l)$ in Eq. (A6). $n_u(V_{BG})$ and $n_l(V_{BG})$ were then determined along with the two fitting parameters $V_{off} = 0.335$ V and $V_{dop} = 0.178$ V using the same procedure as described above.

APPENDIX B: SET ON A BILAYER

Here we show the derivation of Eq. (8). To start with, we calculate the variations of Eqs. (A1)–(A5) by setting $\delta V_{BG} \neq 0$

and $\delta V_{2D} = 0$. This assignment corresponds to the case of applying an ac voltage to the backgate only. We obtain the following relation:

$$\frac{\delta E_1}{\delta V_{BG}} = -\frac{d_u d_l}{D^3}, \tag{B1}$$

where $d_i = \frac{\varepsilon}{e^2}\frac{\partial \mu_i}{\partial n_i}$, $i = u$ or l and $D^3 = l_{FG} l_{BG}(d + d_u + d_l) + d(l_{FG} d_l + l_{BG} d_u) + d_u d_l (l_{FG} + l_{BG} + d)$.

Applying an ac voltage to the two 2DESs only, we set $\delta V_{BG} = 0$ and $\delta V_{2D} \neq 0$ and get

$$\frac{\delta E_1}{\delta V_{2D}} = -\frac{l_{BG}(d + d_u + d_l) + d d_l}{D^3}. \tag{B2}$$

The change of the current δI_{SET} is proportional to δE_1 such that

$$\frac{\delta I_{SET}}{\delta V_{BG}} \left(\frac{\delta I_{SET}}{\delta V_{2D}}\right)^{-1} = \frac{\delta E_1}{\delta V_{BG}} \left(\frac{\delta E_1}{\delta V_{2D}}\right)^{-1}. \tag{B3}$$

Combining the three equations above, one obtains Eq. (8).

By taking the limit $n_l \to 0$, we can check for consistency. As $\partial \mu_l / \partial n_l \to -\infty$ when n_l approaches zero, Eq. (8) now reads

$$\frac{\partial I_{SET}}{\partial V_{BG}} \left(\frac{\partial I_{SET}}{\partial V_{2D}}\right)^{-1} = \frac{d_u}{l_{BG} + d}. \tag{B4}$$

This equation describes the single layer case.

[1] J. P. Eisenstein and A. H. MacDonald, Nature (London) **432**, 691 (2004).
[2] J. P. Eisenstein, G. S. Boebinger, L. N. Pfeiffer, K. W. West, and S. He, Phys. Rev. Lett. **68**, 1383 (1992).
[3] Y. W. Suen, L. W. Engel, M. B. Santos, M. Shayegan, and D. C. Tsui, Phys. Rev. Lett. **68**, 1379 (1992).
[4] I. B. Spielman, J. P. Eisenstein, L. N. Pfeiffer, and K. W. West, Phys. Rev. Lett. **84**, 5808 (2000).
[5] L. Tiemann, W. Dietsche, M. Hauser, and K. von Klitzing, New J. Phys. **10**, 045018 (2008).
[6] T. Hyart and B. Rosenow, Phys. Rev. B **83**, 155315 (2011).
[7] I. B. Spielman, J. P. Eisenstein, L. N. Pfeiffer, and K. W. West, Phys. Rev. Lett. **87**, 036803 (2001).
[8] I. B. Spielman, M. Kellogg, J. P. Eisenstein, L. N. Pfeiffer, and K. W. West, Phys. Rev. B **70**, 081303(R) (2004).
[9] E. Tutuc, M. Shayegan, and D. A. Huse, Phys. Rev. Lett **93**, 036802 (2004).
[10] R. D. Wiersma, J. G. S. Lok, S. Kraus, W. Dietsche, K. von Klitzing, D. Schuh, M. Bichler, H.-P. Tranitz, and W. Wegscheider, Phys. Rev. Lett. **93**, 266805 (2004).
[11] A. R. Hamilton, M. Y. Simmons, F. M. Bolton, N. K. Patel, I. S. Millard, J. T. Nicholls, D. A. Ritchie, and M. Pepper, Phys. Rev. B **54**, R5259 (1996).
[12] A. Sawada, Z. F. Ezawa, H. Ohno, Y. Horikoshi, Y. Ohno, S. Kishimoto, F. Matsukura, M. Yasumoto, and A. Urayama, Phys. Rev. Lett. **80**, 4534 (1998).
[13] V. T. Dolgopolov, A. A. Shashkin, E. V. Deviatov, F. Hastreiter, M. Hartung, A. Wixforth, K. L. Campman, and A. C. Gossard, Phys. Rev. B **59**, 13235 (1999).
[14] E. Tutuc, S. Melinte, E. P. De Poortere, R. Pillarisetty, and M. Shayegan, Phys. Rev. Lett. **91**, 076802 (2003).
[15] S. Q. Murphy, J. P. Eisenstein, G. S. Boebinger, L. N. Pfeiffer, and K. W. West, Phys. Rev. Lett. **72**, 728 (1994).
[16] P. Giudici, K. Muraki, N. Kumada, Y. Hirayama, and T. Fujisawa, Phys. Rev. Lett. **100**, 106803 (2008).
[17] P. Giudici, K. Muraki, N. Kumada, and T. Fujisawa, Phys. Rev. Lett. **104**, 056802 (2010).
[18] W. R. Clarke, A. P. Micolich, A. R. Hamilton, M. Y. Simmons, C. B. Hanna, J. R. Rodriguez, M. Pepper, and D. A. Ritchie, Phys. Rev. B **71**, 081304 (2005).
[19] A. Yacoby, H. F. Hess, T. A. Fulton, L. N. Pfeiffer, and K. W. West, Solid State Commun. **111**, 1 (1999).
[20] L. Tiemann, Y. Yoon, W. Dietsche, K. von Klitzing, and W. Wegscheider, Phys. Rev. B **80**, 165120 (2009).
[21] Y. Yoon, L. Tiemann, S. Schmult, W. Dietsche, K. von Klitzing, and W. Wegscheider, Phys. Rev. Lett. **104**, 116802 (2010).
[22] S. Schmult, L. Tiemann, W. Dietsche, and K. von Klitzing, J. Vac. Sci. Technol. B **28**, C3C1 (2010).
[23] V. Venkatachalam, A. Yacoby, L. Pfeiffer, and K. West, Nature (London) **469**, 185 (2011).
[24] M. Kellogg, J. P. Eisenstein, L. N. Pfeiffer, and K. W. West, Phys. Rev. Lett. **93**, 036801 (2004).
[25] J. P. Eisenstein, L. N. Pfeiffer, and K. W. West, Phys. Rev. B **50**, 1760 (1994).
[26] X. Ying, S. R. Parihar, H. C. Manoharan, and M. Shayegan, Phys. Rev. B **52**, R11611 (1995).
[27] N. K. Patel, I. S. Millard, E. H. Linfield, P. D. Rose, M. P. Grimshaw, D. A. Ritchie, G. A. C. Jones, and M. Pepper, Phys. Rev. B **53**, 15443 (1996).
[28] A. G. Davies, C. H. W. Barnes, K. R. Zolleis, J. T. Nicholls, M. Y. Simmons, and D. A. Ritchie, Phys. Rev. B **54**, R17331 (1996).
[29] A. R. Champagne, A. D. K. Finck, J. P. Eisenstein, L. N. Pfeiffer, and K. W. West, Phys. Rev. B **78**, 205310 (2008).
[30] J. Martin, B. E. Feldman, R. T. Weitz, M. T. Allen, and A. Yacoby, Phys. Rev. Lett. **105**, 256806 (2010).
[31] E. A. Henriksen and J. P. Eisenstein, Phys. Rev. B **82**, 041412 (2010).
[32] G. Fano and F. Ortolani, Phys. Rev. B **37**, 8179 (1988).
[33] S. I. Dorozhkin, R. J. Haug, K. von Klitzing, and K. Ploog, Phys. Rev. B **51**, 14729 (1995).
[34] K. Moon, H. Mori, K. Yang, S. M. Girvin, A. H. MacDonald, L. Zheng, D. Yoshioka, and S.-C. Zhang, Phys. Rev. B **51**, 5138 (1995).
[35] B. Roostaei, K. J. Mullen, H. A. Fertig, and S. H. Simon, Phys. Rev. Lett. **101**, 046804 (2008).
[36] P. R. Eastham, N. R. Cooper, and D. K. K. Lee, Phys. Rev. B **80**, 045302 (2009).
[37] V. S. Khrapai, A. A. Shashkin, M. G. Trokina, V. T. Dolgopolov, V. Pellegrini, F. Beltram, G. Biasiol, and L. Sorba, Phys. Rev. Lett. **99**, 086802 (2007).
[38] S. Ilani, J. Martin, E. Teitelbaum, J. H. Smet, D. Mahalu, V. Umansky, and A. Yacoby, Nature (London) **427**, 328 (2004).
[39] J. Martin, S. Ilani, B. Verdene, J. Smet, V. Umansky, D. Mahalu, D. Schuh, G. Abstreiter, and A. Yacoby, Science **305**, 980 (2004).